Spatial Heterogeneity, Stromal Phenotypes, and Therapeutic Vulnerabilities in Colorectal Cancer Peritoneal Metastasis

Chin-Ann Johnny Ong[1,2,3,4,5,6,7], Joseph J. Zhao[8,9,10,11], Ying Liu[1,2,3], Supriya Srivastava[11], Daryl K.A. Chia[12], Ying En Quek[8], Xiaonan Fan[13], Haoran Ma[10], Kie Kyon Huang[10], Taotao Sheng[14], Qiu Xuan Tan[1,2,3], Gillian Ng[1,2,3], Joey W.S. Tan[1,2,3], Jia-Ying Joey Lee[15,16], Lit-Hsin Loo[15,16], Li Yen Chong[6,17], Xue Wen Ong[10], Su Ting Tay[10], Takeshi Hagihara[10], Angie Tan[10], Craig Ryan Cecil Joseph[6,17], Melissa C.C. Teo[1,2], Josephine Hendrikson[1,2,3], Clara Y.L. Chong[1,2,3], Wanyu Guo[1,2,3], Claramae S. Chia[1,2,4,5], Jolene S.M. Wong[1,2,4,5], Chin Jin Seo[1,2,4,5], Mingzhe Cai[1,2,4,5], Yvonne Tay[13], Kevin M.S. Sim[18], Ryan Y.K. Tay[8], Robert Walsh[9], Marcello Guaglio[19], Federica Morano[19], Ming Teh[11], Huey Yew Jeffrey Lum[18], Tony K.H. Lim[20,21], Louis Vermeulen[22,23,24], Maarten F. Bijlsma[22,23], Kristiaan Lenos[22,23], Samuel J. Klempner[25], Joe P.S. Yeong[6,17], Wei Peng Yong[7,9,13], Filippo Pietrantonio[19], Patrick Tan[7,10,13,14,26], and Raghav Sundar[7,8,9,10,27]

ABSTRACT

Purpose: Peritoneal metastases (PM) in colorectal cancer portend a poor prognosis. We sought to elucidate molecular features differentiating primary tumors (PT) from PMs and actionable targets facilitating transcoelomic dissemination and progression.

Experimental Design: We performed multiomic profiling of 227 samples from 136 patients, including 56 PTs and 120 synchronous PMs comprising 34 matched PT–PM pairs. Whole-exome and bulk RNA sequencing analyses were conducted to identify underlying genomic aberrations and transcriptomic differences between primary and peritoneal lesions. We spatially characterized the microenvironment of tumor–stroma compartments and studied the roles of stromal phenotypes in promulgating tumorigenesis.

Results: Whole-exome sequencing found that genomic alterations and clonality patterns between PTs and PMs remain broadly similar. Transcriptomic profiles, however, suggest a transition as tumors reach the peritoneum toward a more mesenchymal tumor profile and fibrotic tumor microenvironment. Applying spatial profiling, we identify a fibro-collagenous and immune-infiltrated stromal phenotype [stromal cluster (SC) 2] characterized by increased cancer-associated fibroblasts, memory B cells, M2 macrophages, and T-cell exhaustion. These findings were orthogonally validated by multiplex IHC. Patients with SC2 stroma had poorer survival and were characterized by high *SERPINE-1* (*PAI-1*) expression. PMs in patients with SC2 stroma were associated with enriched oncogenic pathways such as TGF-β. PAI-1 inhibition of colorectal cancer PM cell lines with a novel biologic demonstrated reduced IL2–STAT5 and TGF-β pathways and cell death.

Conclusions: Our findings unveil distinctive and actionable molecular signatures, offering deeper insights into the intricate cross-talk between tumor cells and stromal microenvironments enabling PM in colorectal cancer.

Introduction

Colorectal cancer, a leading cause of cancer-related death, often metastasizes to the peritoneum, significantly worsening patient outcomes. For colorectal cancer peritoneal metastases (PM), systemic therapies are inadequate, necessitating novel treatment strategies (1). In the process of transcoelomic metastases, primary tumor (PT) cells undergo a multistep process, including detachment, migration, invasion, and neovascularization facilitated by the tumor microenvironment's (TME) stromal compartment (2–6). Stromal and tumor cells engage in bidirectional cell to cell communication in which tumor cells exploit stroma cells to acquire distinctive cancer hallmarks (7).

Although the role of stroma in tumorigenesis is increasingly recognized, effective therapeutic targeting of the stromal compartment

[1]Department of Sarcoma, Peritoneal and Rare Tumors (SPRinT), Division of Surgery and Surgical Oncology, National Cancer Centre Singapore, Singapore, Singapore. [2]Department of Sarcoma, Peritoneal and Rare Tumors (SPRinT), Division of Surgery and Surgical Oncology, Singapore General Hospital, Singapore, Singapore. [3]Laboratory of Applied Human Genetics, Division of Medical Sciences, National Cancer Centre Singapore, Singapore, Singapore. [4]SingHealth Duke-NUS Surgery Academic Clinical Program, Duke-NUS Medical School, Singapore, Singapore. [5]SingHealth Duke-NUS Oncology Academic Clinical Program, Duke-NUS Medical School, Singapore, Singapore. [6]Institute of Molecular and Cell Biology (IMCB), Agency for Science, Technology and Research (A*STAR), Singapore, Singapore. [7]Singapore Gastric Cancer Consortium, Singapore, Singapore. [8]Yong Loo Lin School of Medicine, National University of Singapore, Singapore, Singapore. [9]Department of Haematology-Oncology, National University Cancer Institute, Singapore, Singapore. [10]Cancer and Stem Cell Biology Program, Duke-NUS Medical School, Singapore, Singapore. [11]Department of Medicine, National University Hospital, Singapore, Singapore. [12]Department of Surgery, National University Hospital, National University Health System, Singapore, Singapore. [13]Cancer Science Institute of Singapore, National University of Singapore, Singapore, Singapore. [14]Genome Institute of Singapore, Agency for Science, Technology and Research, Singapore, Singapore. [15]Bioinformatics Institute (BII), Agency for Science, Technology and Research (A*STAR), Singapore, Singapore. [16]Digital Analytics Laboratory, ImmunoQs Pte. Ltd., Singapore, Singapore. [17]Singapore Immunology Network (SIgN), Agency for Science, Technology and Research (A*STAR), Singapore, Singapore. [18]Department of Pathology, National University Hospital, Singapore, Singapore. [19]Medical Oncology Department, Fondazione IRCCS Istituto Nazionale dei Tumori, Milan, Italy.

Translational Relevance

The discovery of stromal cluster 2, a stromal phenotype tied to poor prognosis, highlights molecular signatures that offer insights into tumor–stromal interactions, potentially leading to therapies targeting the tumor microenvironment in colorectal cancer.

remains conspicuously absent in modern clinical practice for colorectal cancer PM. This stems from a lack of well-defined paracrine signaling targets in colorectal cancer PM, compared with other PM cancers such as in pancreatic or gastric cancer (6, 8–10). Although initial studies have provided some insights, further investigations are needed to identify unique actionable biomarkers within the colorectal cancer PM niche (10–12).

This study aims to address this gap by analyzing the exomes, transcriptomes, and spatial profiles of both cross-sectional and patient matched PT and PM. Our findings unveil distinctive molecular signatures, offering deeper insights into the intricate paracrine communication pathways between the stromal microenvironment and tumor cells that enable PM in colorectal cancer.

Materials and Methods

Tissue samples from patients with colorectal cancer and colorectal cancer PM who underwent surgery at the Singapore General Hospital, National Cancer Centre Singapore, and Fondazione IRCCS Istituto Nazionale dei Tumori of Milan, Italy, between July 2001 and December 2021 were obtained. PT, PM, and adjacent normal tissue were obtained and constructed into two cohorts of tissue microarrays (TMA)—PM tissue samples from patients with colorectal cancer PM and matched PT tissue samples with PM tissue samples from patients with colorectal cancer PM. Patients with colorectal cancer PM who underwent surgery at the Singapore General Hospital and National Cancer Centre Singapore were prospectively recruited between August 2006 and March 2022 (SingHealth Centralised Institutional Review Board reference numbers 2015/2479 and 2020/2145). PT, PM, and adjacent normal tissue were sampled, and clinical data were obtained prospectively. This study was conducted in accordance with ethical principles consistent with the Declaration of Helsinki.

Whole-exome and whole-transcriptome sequencing

For tissue that was rapidly frozen, bulk whole-exome sequencing (WES) and whole-transcriptome sequencing (WTS) analyses were conducted. Briefly, genomic DNA from snap-frozen tissue was extracted using the QIAamp DNA Mini Kit (Qiagen) and subsequently sequenced on the HiSeq platform to generate 150 bp paired-end sequencing reads (NovogeneAIT). Exome sequencing reads were aligned to the reference human genome hs37d5 using BWA-MEM (13). Mutect2 (14) was used in paired mode to generate somatic single-nucleotide variants and indels by comparing BAM files from tumor and matched normal or blood samples. Germline variants were filtered using the gnomAD database, and a panel of normals was generated from all normal samples. Analysis of somatic variants was conducted with the maftools package (15). For RNA sequencing experiments, total RNA was extracted using the RNeasy Mini Kit (Qiagen). Libraries were sequenced on a HiSeq4000 sequencer using the paired-end 150 bp read option. Quality control (QC)–passed reads were aligned to the human reference CGRh38/hg38 genome using STAR v.2.7.9a. Transcript abundance quantification was performed using RSEM v1.3.3 (16).

Spatial profiling—spatial transcriptomics and proteomics

In the case of tissue preserved in formalin-fixed paraffin embedding, spatial profiling was carried out utilizing the NanoString GeoMx digital spatial profiling (DSP) platform for spatial transcriptomics and Lunaphore COMET for spatial proteomics. For NanoString GeoMX, a standard fluorescence-labeled morphology marker panel consisting of pan-cytokeratin for epithelial regions, CD45 for immune cells, α-smooth muscle actin for fibroblast, and nuclear stain was used as region of interest (ROI) selection references. ROIs for each slide were drawn and selected. Data were analyzed by uploading the counts dataset from the Illumina run into the GeoMx DSP analysis suite. Biological probe QC was performed using default settings. For Lunaphore COMET, 4-μm-thick formalin-fixed, paraffin-embedded sections were first subjected to heat-mediated antigen retrieval. Sequential immunofluorescence protocol was then performed on the tissue sections using the COMET platform for the detection of six primary antibodies (aSMA, CD163, CD20, CD3, CD45, and CD68), with subsequent image acquisition. Positive cells for each marker were identified

[20]Department of Anatomical Pathology, Singapore General Hospital, Singapore, Singapore. [21]Pathology Academic Clinical Program, SingHealth Duke-NUS Academic Medical Centre, Singapore, Singapore. [22]Amsterdam UMC Location University of Amsterdam, Laboratory for Experimental Oncology and Radiobiology, Amsterdam, the Netherlands. [23]Cancer Center Amsterdam, Cancer Biology, Amsterdam, the Netherlands. [24]Oncode Institute, Amsterdam, the Netherlands. [25]Division of Hematology-Oncology, Department of Medicine, Massachusetts General Hospital, Boston, Massachusetts. [26]SingHealth/Duke-NUS Institute of Precision Medicine, National Heart Centre Singapore, Singapore, Singapore. [27]The N.1 Institute for Health, National University of Singapore, Singapore, Singapore.

C.-A. J. Ong, J.J. Zhao, and Y. Liu contributed equally and are joint first-authors of this article.

C.-A. J. Ong, P. Tan, and R. Sundar are joint corresponding and senior authors of this article.

Corresponding Authors: Raghav Sundar, National University of Singapore, National University Cancer Institute, 1E Kent Ridge Road, Singapore 119228, Singapore. E-mail: raghav.sundar@yale.edu; Patrick Tan, Duke-NUS Medical School, Genome Institute of Singapore, Agency for Science, Technology and Research (A*STAR), Cancer Science Institute of Singapore, 8 College Road, Singapore 169857, Singapore. E-mail: gmstanp@duke-nus.edu.sg; and Chin-Ann Johnny Ong, Laboratory of Applied Human Genetics, Division of Medical Sciences, National Cancer Centre Singapore, Department of Sarcoma, Peritoneal and Rare Tumors (SPRinT), Division of Surgery and Surgical Oncology, National Cancer Centre Singapore, 30 Hospital Blvd, Singapore 168583, Singapore. E-mail: johnny.ong.c.a@singhealth.com.sg

Clin Cancer Res 2025;31:2515–29

doi: 10.1158/1078-0432.CCR-24-3780

This open access article is distributed under the Creative Commons Attribution-NonCommercial-NoDerivatives 4.0 International (CC BY-NC-ND 4.0) license.

©2025 The Authors; Published by the American Association for Cancer Research

using a web-based hyperplex tissue scoring system (ImmunoThreshold; ImmunoQs Pte. Ltd.) through Gaussian mixture modeling.

Unsupervised clustering of stromal compartments

Unsupervised clustering of DSP-profiled samples was conducted with consensus clustering (17) with the CancerSubtypes (18) workflow. Q3-averaged normalized DSP-NGS GeoMx mRNA expression was utilized. The top 1000 genes of highest variance were utilized. Distances between patients were defined by Canberra distances and clustering was conducted with the partitioning around medoids (PAM) algorithm.

Retrieval of the stromal cluster 2 signature

The stromal cluster 2 (SC2) signature was retrieved by identifying the top 1000 genes of highest variance which were ranked by the sum of t-statistics (unpaired *t* tests) across the following comparisons: SC2 versus SC1, SC2 versus SC3, and SC2 versus tumor ROIs. Only genes with *P*-adjusted values of <0.05 across all three comparisons were included. Top 10 (up- and downregulated) differentially expressed genes were selected. The final composite and bidirectional SC2 signature was retrieved through the singscore (19) package in R.

Methods of A5 discovery and validation

Ascites collection

All patients provided written informed consent according to the study protocol approved by the SingHealth Centralised Institutional Review Board (ref: 2015/2479). Ascitic fluid was collected from the peritoneal cavity at the beginning of cytoreductive surgery (CRS) or during routine paracentesis and subjected to centrifugation at 2,000 *g* for 10 minutes to remove cellular components. The fluid component was then filter-sterilized using the 0.22 μm filter and stored at −80°C.

Cell line

Colo-205, a human colorectal cell line representative of PM, was purchased from ATCC (CCL-222) in November 2015 and cultured in RPMI-1640 with 10% FBS (HyClone, SV30160) supplemented with 100 U/mL penicillin and 100 μg/mL streptomycin (HyClone, SV30010) at 37°C with 5% CO_2. Cell line authentication was performed by ATCC via short tandem repeat profiling. Before experiments, Colo-205 cells were starved overnight in serum-free RPMI medium (SFM). The cells were maintained in culture for no more than 20 passages and/or less than 6 months following retrieval from liquid nitrogen storage and were free from *Mycoplasma* as tested using the MycoAlert Mycoplasma detection kit (Lonza, LT07-318).

Animal

All mice experiments were carried out according to the protocol approved by the SingHealth Institutional Animal Care and Use Committee (ref: 2020-/SHS/1610). All mice used in this study were 6- to 9-week-old NCr nude mice purchased from InVivos (CrTac:NCr-Foxn1^{nu}). Mice were provided Teklad global 18% protein rodent diet (Envigo) and water *ad libitum*.

Antibody discovery by phage display

Phage display was performed to screen for antibodies from the single-chain antibody variable fragment (scFv) human-naïve LiAb-SFMAX library generated from 368 healthy donors of five ethnic groups (ProteoGenix). Briefly, a 50% to 50% mixture of stable active (Innovative Research, IHUPAI1RSM1MG) and latent (Innovative Research, IHUPAI1RWTL1MG) forms of human PAI-1 recombinant protein was used as antigens to attract phages that recognize PAI-1 in four subsequent biopanning rounds. ELISA was performed with elution of each round on the PAI-1 mixture to evaluate their recognition of PAI-1. The specificity of 240 monoclonal phages from the selected elution to the PAI-1 mixture, active PAI-1, and latent PAI-1 was evaluated by ELISA. Subsequently, competitive ELISA was performed to screen for phages capable of competing with PAI-1 small-molecule inhibitors (50%–50% mix of TM5441 and tiplaxtinin). Eventually, one phage sequence was identified and expressed in the format of IgG kappa in the Chinese hamster ovary cells. The endotoxin-removal process was performed on the antibody to reach <1 EU/mL for the *in vitro* and *in vivo* experiments.

Western blotting

A total of 100 ng of active (Innovative Research, IHUPAI1ARWT1MG), stable active, and latent forms of PAI-1 recombinant proteins were denatured at 97°C for 5 minutes and resolved in 12% polyacrylamide gels in Tris/glycine/SDS running buffer (24.76 mmol/L Tris, 191.83 mmol/L glycine, and 0.1% SDS), followed by transfer to 0.45 μm nitrocellulose membranes (Bio-Rad, 1620115) in Tris/glycine/methanol transfer buffer (24.76 mmol/L Tris, 191.83 mmol/L glycine, and 20% methanol). Precision Plus Protein Dual Color Standards (Bio-Rad, #1610374) was used as the protein ladder. The following steps were performed at room temperature. The membranes were blocked with 5% non-fat milk in 1× PBS containing 0.1% Tween 20 (PBST) for 1 hour before blotting with 1 μg/mL A5 antibody, 1 μg/mL unspecific human IgG (Sigma, I5154), or 1:10,000 rabbit anti–PAI-1 antibody (Cell Signaling Technology, 11907) for 2 hours. After four washes (5 minutes per wash) in PBST, the membranes were blotted with 1:5,000 peroxidase anti–human IgG antibody (Jackson ImmunoResearch, 109-035-003) or 1:5,000 anti–rabbit horseradish peroxidase–conjugated antibody (GE Healthcare, NA934) for 30 minutes. After another four washes in PBST, the membranes were incubated with SuperSignal West Dura Substrate (Thermo Fisher Scientific, 34076) for 5 minutes and the signals were captured by the ChemiDoc imaging system (Bio-Rad).

PAI-1 neutralization assay

The PAI-1 function in inhibiting tissue-type plasminogen activator (tPA) activity was assessed by the PAI-1 Activity Assay Kit (Abcam, ab283368). In a 100 μL reaction, 300 ng/mL stable active PAI-1 was incubated with 1 μg A5, 1 μg unspecific human IgG (Sigma, I5154), or PBS vehicle for 60 minutes at 37°C. Then 20 μL of this mixture was incubated with 20 μL of 40 U/mL tPA supplied in the kit at room temperature for 20 minutes. The rest steps followed the manufacturer's instructions. Triplicates were performed for statistical analyses.

The PAI-1 function in inhibiting urokinase-type plasminogen activator (uPA) activity was assessed by the uPA Activity Assay Kit (Merck, ECM600). In a 200 μL reaction, 100 ng stable active PAI-1 was incubated with 1 μg A5, 1 μg unspecific human IgG (Sigma, I5154), or PBS vehicle for 60 minutes at 37°C. Then 150 μL of this mixture was incubated with 10 μL uPA supplied in the kit. The rest steps followed the manufacturer's instructions. Triplicates were performed for statistical analyses.

Nuclear magnetic resonance spectroscopy

19F nuclear magnetic resonance (NMR) spectroscopy was obtained on a Bruker 400 MHz equipped with a BBO probe at 25°C

(Bruker Instruments). In a 500 μL reaction, 75 μmol/L tiplaxtinin was incubated with 3.2 μmol/L stable active PAI-1 in PBS buffer for 20 minutes at room temperature. In the sample, 0.00067% 1,1,1-trifluoroacetate and 10% D_2O were included and used as the chemical shift reference and lock reagent, respectively. The NMR spectra of tiplaxtinin in the absence and presence of 10 μg A5 were collected by standard 1D 19F-NMR. The parameters for data acquisition were the number of scans of 128, the spectra width of 80 parts per million, the sample temperature of 298k, the delays of 1 second, and the middle point of spectrum at −80 parts per million. The data were baseline-corrected and axis-calibrated using Topspin (Bruker, version 4.0.9).

In vitro proliferation inhibition

In 96-well plates, 5,000 Colo-205 cells/well were seeded in technical triplicate and were grown in SFM supplemented with 5% ascites or SFM supplemented with 10% FBS for 24 hours, followed by the treatment with 150 μg/mL A5, 150 μg/mL unspecific human IgG (Sigma, I4506), or PBS vehicle for 72 hours at 37°C. Cell viability was then determined by the CellTiter-Glo assay (Promega, G7570). Cell viability was normalized to the PBS control and statistical analyses were performed on biological triplicates.

STAT3 inhibition assay

In 12-well plates, 8×10^5 Colo-205 cells/well were seeded and incubated in SFM supplemented with 5% ascites and various concentrations of A5, unspecific human IgG (Sigma, I4506), or PBS vehicle for 16 hours at 37°C. The harvested cells were lysed with lysis buffer (Cell Signaling Technology, 9803S) in the presence of protease and phosphatase inhibitors (Thermo Fisher Scientific, 1861281), followed by total protein concentration measured by Bradford protein assay (Bio-Rad, 5000006). Then 25 μg of the protein lysate was used to measure total STAT3 and p-STAT3 (Tyr705) by ELISA using the PathScan Total Stat3 Sandwich ELISA kit (Cell Signaling Technology, 7305C) and the PathScan Phospho-Stat3 (Tyr705) Sandwich ELISA kit (Cell Signaling Technology, 7300C), respectively. All samples were measured in two technical replicates as per the manufacturer's instructions. Biological triplicates were performed for statistical analyses.

Transcriptome sequencing

In 12-well plates, 8×10^5 Colo-205 cells/well were seeded and incubated in SFM supplemented with 5% ascites and 100 μg/mL of A5 or 100 μg/mL unspecific human IgG (Sigma, I4506) for 24 hours at 37°C in two biological replicates. The total RNA was extracted using the AllPrep RNA/DNA/miRNA Universal kit (Qiagen, 80224). Total RNA libraries were generated using TruSeq Stranded Total RNA with Ribo-Zero H/M/R_Gold (Illumina) and then sequenced on the Illumina NovaSeq platform at paired-end 151 bp. Expression profiles were calculated for each sample and transcript/gene as read count, fragment per kilobase of transcript per million mapped reads, was used for downstream analyses.

Other statistical methods and reproducibility

Survival analysis was conducted using a multi-variate Cox proportional hazards model with the *survival* package in R. The median follow-up time was retrieved using the reverse Kaplan–Meier method with the *prodlim* package in R. A two-sided *t* test was used for continuous variables with normal distributions, and a two-sided Wilcoxon test was used for non-normally distributed variables. ANOVA was used for comparisons between multiple groups. The Fisher exact test was applied to unpaired count data, and the McNemar test was applied to paired data.

Further details are reported in the Supplementary Methods S1. All analyses were undertaken in R-4.2.0. A two-sided *P* value of less than 0.05 was considered statistically significant.

Data availability

The genomic and transcriptomic data have been deposited at the European Genome-phenome Archive under accession number EGAS50000000813. Other data used in this study are available on request. Correspondence and requests for materials should be addressed to Raghav Sundar, Patrick Tan, or Chin-Ann Johnny Ong. The code utilized in this study is publicly available in the following Github repository: github.com/josephjzhao/crcpm.

Results

Cohort overview

Peritoneal tissue samples were predominantly collected during diagnostic laparoscopies or laparotomies and oncological surgical resections including CRS and hyperthermic intraperitoneal chemotherapy (HIPEC). One hundred and thirty-six patients with synchronous colorectal cancer PM were recruited. The median age was 54.00 years (IQR, 45.90–63.38) and the majority were female (66.9%), Chinese (71.8%), and advanced PT (T4 tumor, 70.1%; N2 tumor, 44.7%). The median peritoneal carcinomatosis index score was 11 (Supplementary Table S1A). From these patients, a total of 227 samples, comprising 56 colorectal cancer PT and 120 PM samples were included (**Fig. 1A** and **B**). A total of 34 patients had paired PT–PM samples. Further information on the availability of paired samples is reported in Supplementary Table S1B and S1C.

Clonality and shared genomic alterations in primary and peritoneal metastatic colorectal cancer

WES was performed on 25 PT and 43 PM colorectal cancer samples from 30 patients to assess differences in genomic landscapes and clonality patterns. The most frequently mutated genes in our cohort included tumor suppressor genes *TP53* (51%) and *APC* (38%), oncogene *KRAS* (26%), and tumor suppressor gene *SMAD4* (18%; **Fig. 1C**; Supplementary Fig. S1). In line with previous reports (20–22), a relatively lower proportion of APC mutations were found in PM samples (**Fig. 1C**). In contrast to previous reports by Stein and colleagues (21), no significant differences were found in the frequency of driver mutations between PT and PM. Notwithstanding, it is worth noting that a lower proportion of *SMAD4* (OR = 0.344, $P = 0.108$), *NBEA* (OR = 0.306, $P = 0.132$), and *RNF43* (OR = 0.400, $P = 0.409$) mutations were found in peritoneal tumors and a higher proportion of *HSPG2* (OR = 3.829, $P = 0.248$) mutations were found in PM, although these comparisons did not reach statistical significance (**Fig. 1D**). Consistent with previous reports by Stein and colleagues (21), no significant differences in tumor mutational burden ($P = 0.708$) were found. Likewise, no significant differences in the fraction of altered genome compartments ($P = 0.810$), median minor allele frequency ($P = 0.860$), whole-genome duplication ($P = 0.736$), and clonality ($P = 1.000$) were found (**Fig. 1E**). These findings suggest that through the process of transcoelomic PMs, tumor cells remain largely clonal in origin, arising from the same ancestral cell as the PT. This may indicate that the metastatic process may not have involved significant additional driver mutations or suggest a phenomenon in which

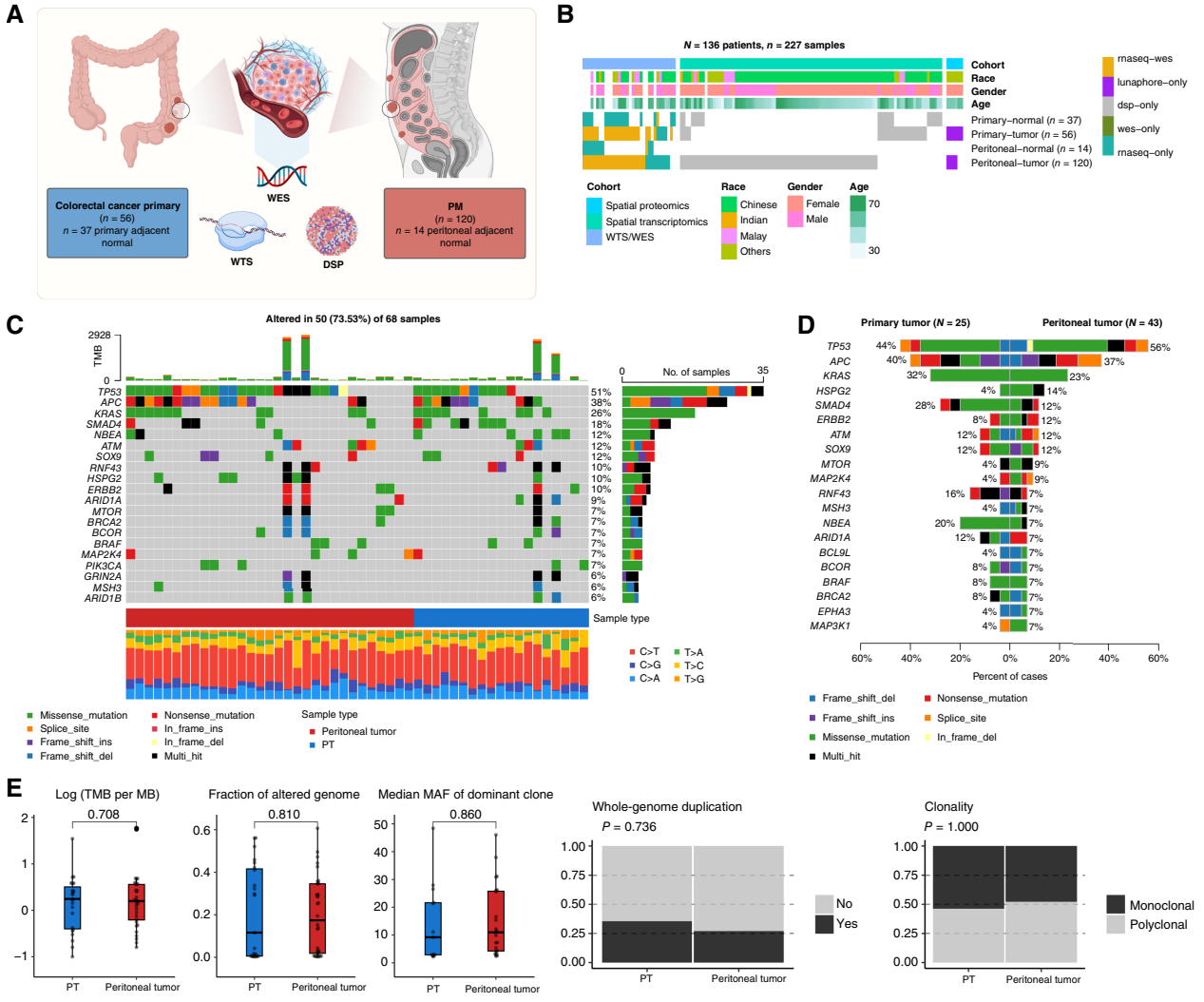

Figure 1.

Cohort overview and genomic evolution between primary and peritoneal tumors. **A,** Graphical summary of samples retrieved in the cohort and assays utilized. **B,** Sample location and assay type overview of cohort. **C,** Oncoprint of genomic aberrations identified. Genes shown here were previously reported by Household and colleagues (22). **D,** Co-bar plot comparison between PT and PM in colorectal cancer. All comparisons were not statistically significant. **E,** PT–PM comparisons of TMB, fraction of altered genome, median MAF of dominant clone, whole genome duplication and clonality. MAF, minor allele frequency. [Created in BioRender. Sundar, R. (2025), https://BioRender.com/y53n114.]

tumor cells evolved linearly with clonal dominance (23). This lack of genomic divergence between PT and PM, despite the differing peritoneal organotropism, motivated our investigation of the TME and gene expression patterns using WTS.

Transcriptional landscape of colorectal cancer PM reveals niche adaptation and microenvironmental remodeling

WTS was conducted on 28 PT, 44 PM, 18 primary normal, and 14 grossly uninvolved peritoneal normal (PMN) samples from 34 patients. In contrast to the broadly similar PT/PM genomic landscapes revealed by WES, we appreciated greater distinction across gene expression profiles, suggesting greater involvement of transcriptional reprogramming in the metastatic process (**Fig. 2A**). Pathways such as IL6–JAK–STAT3 signaling, TGF-β, and angiogenesis were found to be significantly enriched in PM (**Fig. 2B**; Supplementary Table S2A). This suggests an active TME with potential roles in supporting tumor cell survival and growth in the peritoneal cavity. Analysis of cell type proportions using various deconvolution algorithms (CIBERSORT/xCell) revealed significant increases in M2 macrophages, endothelial cells, myeloid dendritic cells, and cancer-associated fibroblast (CAF) proportions in peritoneal tumors. Conversely, plasma B cells and memory resting $CD4^+$ T cells were reduced in peritoneal tumors (**Fig. 2C**). These changes are consistent with a more immunosuppressive and pro-angiogenic TME in the peritoneal cavity, potentially facilitating metastasis.

We also found that as tumor samples transition toward the peritoneum, samples become increasingly mesenchymal [epithelial–mesenchymal transition (EMT) score (24), $P = 0.02$] and have lower tumor purity scores [ESTIMATE (25) algorithm, $P = 0.0026$]. Consistent with previous reports by Lenos and colleagues (20), a

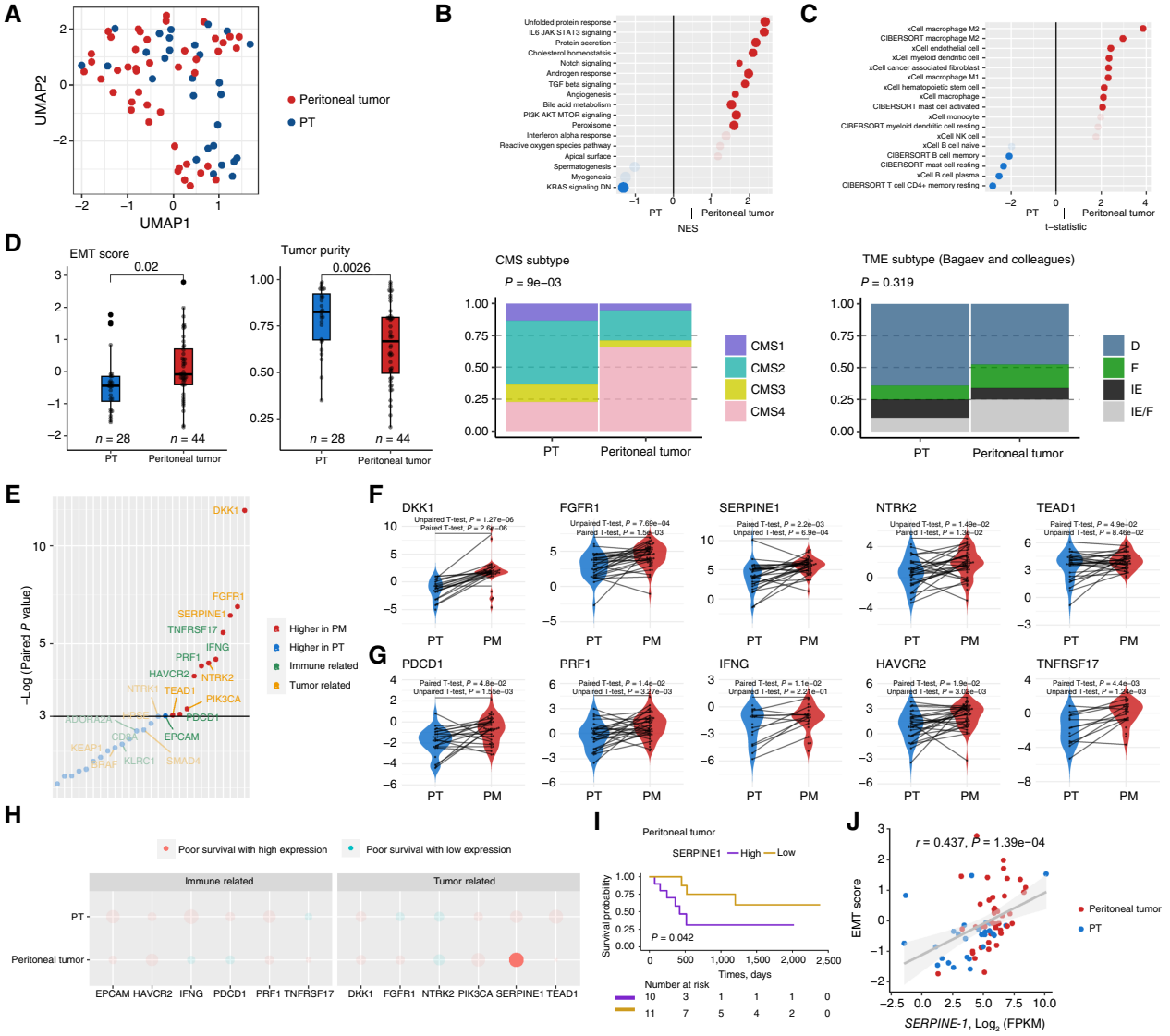

Figure 2.

Transcriptomic and microenvironmental evolution in transcoelomic metastasis. **A,** UMAP of gene expression profiles of primary and peritoneal tumor samples in colorectal cancer (PT, $n = 28$; PM, $n = 44$). **B,** Gene set enrichment analysis pathway changes between primary and peritoneal tumor samples (PT, $n = 28$; PM, $n = 44$). Pathways were shown if |NES| was greater than 1.00. Pathways were highlighted if adjusted P values were less than 0.05. **C,** Immune deconvoluted cell subtypes by xCell and CIBERSORT (PT, $n = 28$; PM, $n = 44$). Comparisons were undertaken with an unpaired t test. Immune cells were shown if |t-statistic| was greater than 1.75. Immune cells were highlighted if P values retrieved from an unpaired t test were less than 0.05. **D,** Differences in EMT score (24), tumor purity [ESTIMATE (25) algorithm], CMS (26, 27) subtype, and TME subtype (PT, $n = 28$; PM, $n = 44$; ref. 28). **E,** Ranked analysis of putative targets in paired PT–PM comparisons. Genes were highlighted if $P < 0.05$ on a paired t test. **F,** Violin plots of tumor and (**G**) immune-related putative therapeutic targets in colorectal cancer PM (unpaired: PT $n = 28$ and PM $n = 44$; paired: PT $n = 27$ and PM $n = 36$). **H,** Overview of prognostic significance (overall survival) of identified putative targets. When patients had more than one sample, the mean gene expression was utilized. P values were retrieved from the log-rank test. The cohort (high vs. low) was dichotomized by median gene expression. **I,** Kaplan–Meier plots of *SERPINE-1* expression vs. overall survival in primary and peritoneal tumor samples. **J,** Scatter plot of EMT score and *SERPINE-1* gene expression. The relationship was assessed using Pearson correlation. CMS, consensus molecular subtype; F, fibrotic; FPKM, fragment per kilobase of transcript per million; IE, immuno-enriched; NES, normalized enrichment score; UMAP, Uniform Manifold Approximation and Projection for Dimension Reduction.

greater proportion of consensus molecular subtypes (refs. 26, 27) 4 (mesenchymal) subtype ($P = 0.009$) were found among peritoneal samples. Peritoneal samples were characterized by prominent TGF-β activation, stromal invasion, and angiogenesis among PM samples. We also noted a trend toward PM samples more likely to be characterized with a fibrotic or an immune-enriched/fibrotic TME (**Fig. 2D**). These TME subtypes were previously described to have dense collagen formation, stromal content, and poor prognosis (Supplementary Table S2B; ref. 28). Although these differences could be partly attributed to sampling bias (in which PT biopsies were more enriched in epithelial cells whereas PM biopsies were more fibrotic), the WTS data suggest a potential role for TME remodeling in PM.

To better understand the inherent phenotype of the grossly uninvolved peritoneum, we also compared PM to PMN. As anticipated, we identified enrichment of several oncogenic pathways when comparing PM to adjacent PMN samples. The enrichment of MTORC1 signaling, E2F targets, the G_2–M checkpoint, stem cell pathways, and TGF-β signaling in PM highlights the aggressive proliferative nature of metastatic cells (Supplementary Fig. S2A). On immune deconvolution, we found a corresponding increase in CD4 T cells, M1 and M2 macrophages, and plasmacytoid dendritic cells within PM (Supplementary Fig. S2B). However, CAFs and endothelial cells, which were previously identified to be enriched in PM when compared with PT, were found to be even greater in adjacent PMN samples compared with PM. To further investigate this, we compared the adjacent PMN samples ($n = 14$) against six benign PMN samples retrieved from patients with nonmalignant and non-infectious conditions (primary diagnoses detailed in Supplementary Table S2C; ref. 6). We found that the corresponding increased preponderance of CAFs and endothelial cells was not observed in these benign PMN samples (Supplementary Fig. S2C and S2D). Together, these data suggest a process in which the grossly uninvolved peritoneum also undergoes remodeling to create a supportive niche for colorectal cancer PM, primarily driven by endothelial cells and CAFs. This phenomenon emphasizes the dynamic interactions within the peritoneum microenvironment that support metastasis.

Clinically relevant genes of interest in colorectal cancer PM

We inspected several clinically relevant tumor and immune-related genes of interest with therapeutic relevance, comparing expression levels between PT and PM. Twelve genes (six tumor-related and six immune-related) were identified to be differentially expressed between PT and PM on paired analyses (**Fig. 2E**, full list of genes in Supplementary Table S2D). Notable examples are *DKK1* (dickkopf WNT signaling pathway inhibitor 1), known as an antagonist of the Wnt/β-catenin signaling pathway, which was found to have significantly higher expressions in PM samples (paired *t* test, $P = 2.6e{-}06$). Likewise, *SERPINE-1* (or *PAI-1*), known for its involvement in remodeling of the colon cancer microenvironment and the infiltration of immune cells via the Notch pathway (29), was found to have significantly higher expressions in PM samples (paired *t* test, $P = 6.9e{-}04$). Other notable tumor-related genes with higher expressions in PM samples include *FGFR1*, *NTRK2*, and *TEAD1* (**Fig. 2F**). Among the immune-related targets, higher expression of *PDCD1* (or *PD-1*), *PRF1*, *IFNG*, *HAVCR2*, and *TNFRSF17* was found in PM samples (**Fig. 2G**).

We evaluated whether gene expression profiles of these differentially expressed genes had a prognostic significance. Patients with high *SERPINE-1* expression in peritoneal tumors were associated with poorer survival (HR = 4.01, log-rank, $P = 0.042$). A similar trend toward poorer survival was observed in patients with high *SERPINE-1* expression in PT samples as well, although this was not statistically significant (HR = 2.48, log-rank, $P = 0.28$; Supplementary Fig. S2E). In a similar cohort of patients with colorectal cancer PM by Lenos and colleagues (20), patients with higher PAI-1 expression in PM samples were also found to have poorer survival (HR = 2.20, $P = 0.047$; Supplementary Fig. S2F). In the same vein, patients with high *SERPINE-1* expression in The Cancer Genome Atlas (TCGA) COAD cohort were found to have poorer survival, although this did not reach statistical significance (HR = 1.42, $P = 0.14$; Supplementary Fig. S2G). No significant survival differences were found with the other identified gene targets (**Fig. 2H** and **I**). *SERPINE-1* was also found to be significantly associated with EMT scores (Pearson r = 0.437, $P = 1.39e{-}04$), in which samples with higher *SERPINE-1* expression were more mesenchymal (**Fig. 2J**).

Microenvironmental convergence at spatial resolution between PT–PM

To further dissect the interplay between tumor cells and the surrounding stroma, we also performed spatial profiling, aiming to investigate gene expression programs specifically within the tumor and stromal compartments of both PT and PM. A total of 342 spatially resolved ROIs from 96 patients were analyzed with NanoString GeoMx DSP (**Figs. 1B** and **3A**). QC parameters were reported in Supplementary Table S3A. Hematoxylin and eosin (H&E) staining was performed from each TMA block, and a pathologist (S. Srivasava) delineated specific ROIs, including tumor, stroma, and normal for each tissue core within the TMA map. The initial pathologist readings were verified by a second pathologist (M. Teh). The adjacent slide was processed using the GeoMx Human Whole Transcriptome Atlas protocol (NanoString). ROI selection was guided by immunostaining with four markers: DNA, CD45, pan-cytokeratin, and smooth muscle actin. A median of 37 ROIs (IQR, 32–38) was selected from a total of nine TMA slides. A total of 269 ROIs (181 tumor and 88 stroma) from PM samples, 45 ROIs (34 tumor and 11 stroma) from PT samples, and 28 (all stroma) ROIs from primary normal samples were retrieved and profiled.

Uniform Manifold Approximation and Projection analysis of DSP ROIs demonstrated clear segregation of tumor and stromal compartments from primary adjacent normal ROIs. Interestingly, compartment specific overlap (tumor and stroma) was seen between PT and PM (**Fig. 3B**). Between stromal and tumor compartments, CD8 T cells, CD4 T cells, and neutrophils were higher in tumor compartments whereas fibroblasts, macrophages, endothelial cells, B cells, and NK were higher in stromal compartments (**Fig. 3C** and **D**). The immune cell type changes found between tumor and stromal compartments were shown to be concordant between primary and peritoneal samples (Pearson r = 0.963, $P < 0.001$; **Fig. 3D**). The spatially resolved patterns of similarity in the microenvironment of PT and PM tumors reflect hypotheses previously suggested by Cambria and colleagues (30), in which physical adaptations conducive to metastasis persist as cellular mechanical memory during the metastatic journey, enhancing the ability of tumor cells to exit blood vessels, survive, and establish themselves in distant organs. These immune cell types were also consistent with changes identified in our earlier WTS PT–PM comparisons, reinforcing their likely role in transcoelomic metastasis.

We validated these findings with spatial multiplex IHC (mIHC; **Fig. 3E**). A total of 773,803 cells were retrieved from 495 ROIs from 10 slides ($n = 6$ PT and $n = 4$ PM) from six patients. Retrieval of cell types is described in the Supplementary Methods in the Spatial Proteomics – Lunaphore COMET section. A total of 525,859 immune cells were retrieved with minimal overlap found (Supplementary Table S3B; Supplementary Fig. S3A and S3B). Consistent with the TME convergence phenomenon shown in our DSP data, compartment-specific PT–PM comparisons of cell type proportions were broadly consistent (**Fig. 3F**) with spatial coordinate information surrounding the tumor stromal interface. We observed increased CD163 macrophages in peritoneal stromal compartments, reduced CD68 macrophages in peritoneal tumor compartments, and reduced T cells within stromal compartments of peritoneal samples. There is a relative increase in fibroblast infiltration within

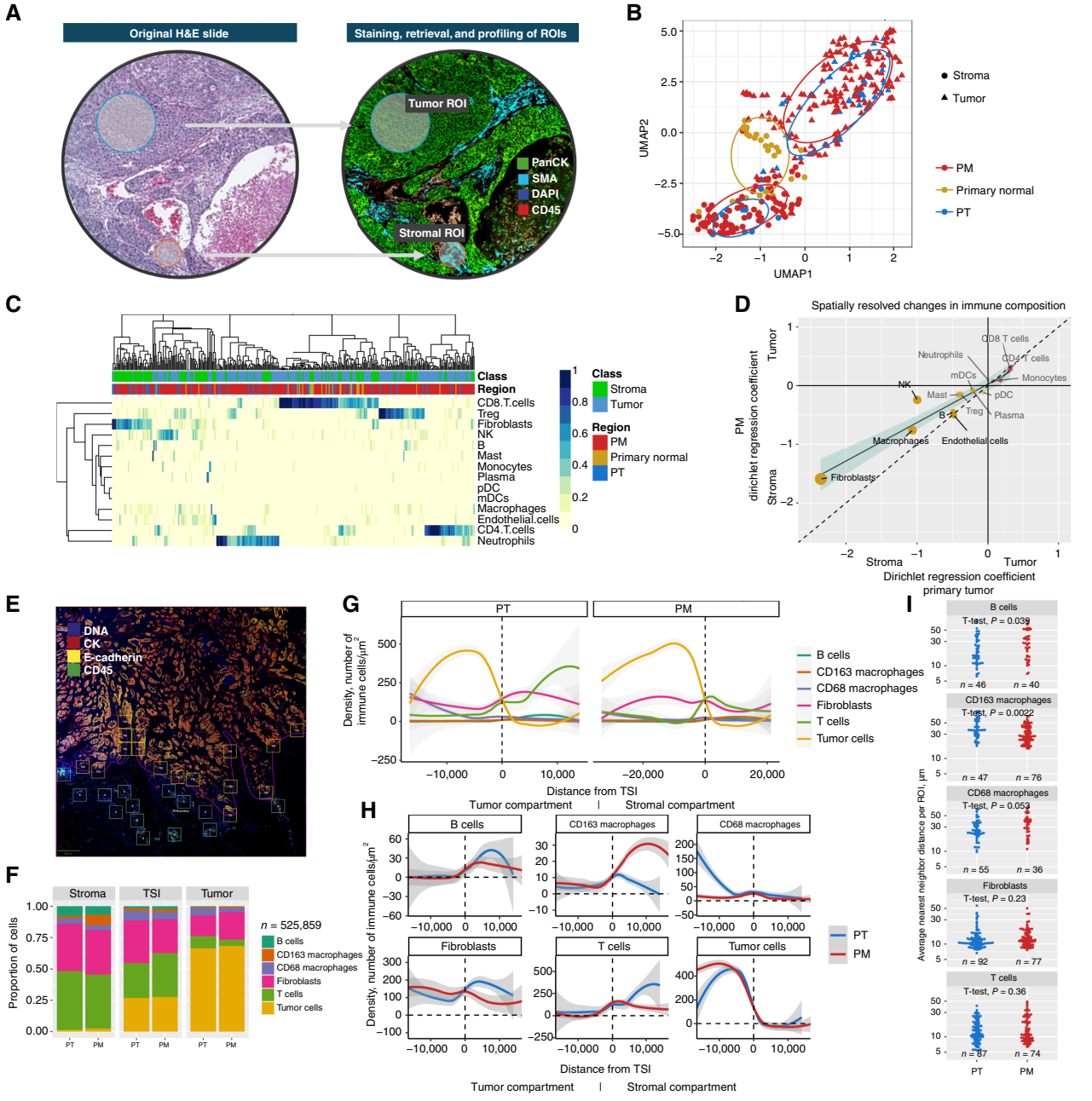

Figure 3.

Microenvironmental convergence between PT–PM. **A,** Illustration of DSP ROI retrieval with NanoString GeoMx. **B,** UMAP of spatially resolved ROIs in CRC PM. **C,** Heatmap of SpatialDecon (31) enumerated immune cell types. **D,** Scatter plot of immune cell type comparisons between tumor–stromal compartments in PT and PM. Immune cell types were highlighted if $P < 0.05$ from the Dirichlet regression model in either comparison. **E,** Illustration of COMET Lunaphore mIHC. **F,** Stacked barchart of cell type proportions stratified by ROI location (stroma vs. TSI vs. tumor) and site (PT vs. PM). **G,** Immune cell type density curves against distance from TSI stratified by PT vs. PM. **H,** Immune cell type density curves against distance from TSI stratified by immune cell types. Tumor compartments were taken to be at negative distance whereas stromal compartments were taken to be at a positive distance from the TSI. Smoothed conditional means density curves were retrieved with the geom_smooth() function in *ggplot2*. **I,** Average immune cell type–specific nearest neighbor distance per ROI stratified by immune cell types across PT vs. PM. Only ROIs with >100 cells per immune cell type were included. mDC, myeloid dendritic cell; PanCK, pan-cytokeratin; pDC, plasmacytoid dendritic cells; Treg, regulatory T cell; TSI, tumor stromal interface; UMAP, Uniform Manifold Approximation and Projection for Dimension Reduction.

peritoneal tumor compartments compared with PT compartments (**Fig. 3G** and **H**). Furthermore, we observed a significantly increased proportion of exhausted cytotoxic T cells ($CD8^+$PD-L1+, PM: 14.5% vs. PT: 2.6%; χ^2 test, $P < 2.2e{-}16$) and regulatory T cells ($CD4^+$-FOXP3+, PM: 28.7% vs. PT: 18.2%; χ^2 test, $P < 2.2e{-}16$) within tumor compartments of PM versus PT (Supplementary Fig. S3C).

We also inspected the degree of cell-specific clustering, reflected by the average nearest neighbor distance per ROI, and found that compared within stromal compartments, B cells ($P = 0.039$) and CD68 macrophages ($P = 0.053$) in peritoneal stromal compartments were more dispersed compared with PT stromal compartments. Conversely CD163 macrophages were more clustered in PM ($P = 0.0022$; **Fig. 3I**). These findings underscore that although broad cell type distributions were converged between PT–PM, some degree of cell subtype spatial heterogeneity is appreciated.

Spatially resolved stromal phenotypes in colorectal cancer PM

Considering the differential immune cell proportions within the tumor and stroma compartments, we sought to further delineate stromal phenotypes of colorectal cancer PM. We selected stroma ROIs and performed consensus clustering, identifying three distinct clusters of stromal ROIs [stromal cluster 1 (SC1) $n = 58$; SC2 $n = 36$; and SC3 $n = 19$; **Fig. 4A**; Supplementary Fig. S4A and S4B]. SC3 was found to predominantly comprise primary normal stroma, whereas SC1 and SC2 had a mix of primary and peritoneal ROIs, with SC2 having a greater proportion of peritoneal samples (91.7% vs. 77.6%; **Fig. 4B**). After excluding patients with only tumor ROIs ($n = 37$, no profiled stromal ROI available), minimal intrapatient stroma cluster heterogeneity was noted, with only nine (15.3%) patients displaying two or more stromal clusters (**Fig. 4C**). We found that patients with SC2, regardless of sample site, were significantly associated with poorer overall survival (log-rank, $P = 0.036$; **Fig. 4D**). For patients with SC2 in PM alone, a trend toward poorer overall survival was appreciated (log-rank, $P = 0.10$; Supplementary Fig. S4C). Conversely, no significant association was found between SC2 and survival among patients with SC2 in PT alone (log-rank, $P = 0.39$). Notwithstanding, survival analysis of the PT subgroup was difficult to interpret in view of the small number of patients ($n = 7$; Supplementary Fig. S4D). On gross inspection of H&E slides of stromal ROIs, we found that histologic features of fibro-collagenous stroma (SC1 50.0% vs. SC2 75.0%, $P = 0.019$) and the presence of inflammatory immune cells (SC1 3.4% vs. SC2 25.0%, $P = 0.002$) were more commonly noted in SC2 compared with SC1 ROIs. SC1 also had a higher proportion of grossly bland stroma on H&E inspection as compared with SC2, although this did not reach statistical significance (15.5% vs. 5.6%, $P = 0.195$; **Fig. 4E**; Supplementary Table S4).

Characteristics of SC2 stromal compartments

Consistent with gross histologic appearances, several inflammatory pathways such as the IL6–JAK–STAT3, IL2–STAT5, and TGF-β were enriched in SC2. EMT scores were also higher in SC2 compared with other stromal phenotypes and tumor compartments (**Fig. 4F**). SC2 ROIs were characterized by increased fibroblasts, macrophages, myeloid dendritic cells, and B cells (31). Conversely, CD4 and CD8 T cells were found to be decreased in SC2 ROIs (**Fig. 4G**). We further inspected cell subtypes with previously described signatures of CAF subtypes (32), B-cell subtypes (33), and macrophage subtypes (34). Specifically, we found that gene set variation analysis scores of B memory cells and M0 and M2 macrophages were uniquely higher in SC2 compartments whereas a majority of CAF subtypes were higher in SC2. We also found that T-cell exhaustion signatures (35) were higher in SC2 compartments (Supplementary Fig. S4E). Gene expression profiles of *SERPINE-1* were specifically high in SC2 stroma (**Fig. 4H**). Consistent with the upstream WTS findings, *SERPINE-1* expression was associated with gene set variation analysis EMT enrichment scores (Pearson r = 0.483, $P = 6.06e{-}08$; **Fig. 4I**). The TGF-β signaling pathway, recognized as a key player in PT–PM WTS comparisons, was found to be enriched in tumor compartments from patients with SC2 stroma in contrast to those without SC2. Other pathways such as the TNF-α, hypoxia, and JAK–STAT were also enriched but these did not reach statistical significance. Conversely, p53 and PI3K pathway activity was found to be significantly lower (**Fig. 4J**).

By inspecting mIHC retrieved immune cell type densities across ROIs, we confirmed a similar phenomenon in which two distinct stromal clusters were found—one being fibroblast infiltrated but T-cell depleted (SC2-like, $n = 67$ ROI) and another which is T-cell infiltrated but fibroblast depleted (SC1-like, $n = 104$ ROI; **Fig. 4K**). There was no significant difference between distance from the tumor stromal interface between stromal phenotypes in both PT and PM (t test, PT $P = 0.65$; PM, $P = 0.20$; Supplementary Fig. S4F). In contrast to what we identified in the DSP data, we note that a higher proportion of SC2-like stromal ROIs conversely originated from PT (χ^2 test, $P = 0.036$, Supplementary Fig. S4G). We demonstrate diverging spatial distributions of T cells and fibroblasts between SC1 and SC2-like stroma. Between both PT and PM, we find close clustering of T cells in SC1-like stromal compartments (t test, PT: $P = 4.2e{-}11$; PM, $P = 4.1e{-}07$) and fibroblasts in SC2-like stromal compartments (t test, PT: $P = 1.9e{-}05$; PM, $P = 5.5e{-}04$; **Fig. 4L** and **M**).

Prognostic significance of the SC2 phenotype

Next, a 20-gene composite and bidirectional SC2 signature (**Fig. 5A**; Methods: Retrieval of the SC2 signature) was curated by collating top differentially expressed genes (both up- and down-regulated) between SC2 versus SC1, SC2 versus SC3, and SC2 versus tumor ROIs (Supplementary Table S5). The SC2 signature demonstrates good internal validation in discriminating SC2 from other compartments (**Fig. 5B** and **C**). We applied the SC2 signature in a parallel colorectal cancer PM cohort described by Lenos and colleagues (20). Patients with a high SC2 signature were likewise found to have poorer survival (log-rank, $P = 0.041$) and higher expression of *SERPINE-1* (t test, $P = 1.3e{-}07$). A subgroup survival analysis of only peritoneal samples from Lenos and colleagues demonstrated a similar trend, although statistically significance was not reached (log-rank, $P = 0.15$; Supplementary Fig. S5). Similar findings were also seen in other colorectal cancer cohorts of PT samples (Q1 vs. Q4 comparisons: TCGA (36), log-rank $P = 0.004$; Gallois and colleagues (37), log-rank $P = 0.086$), along with corresponding higher expressions of *SERPINE-1* (TCGA, $P < 2.2e{-}16$; Gallois and colleagues, $P = 0.049$; **Fig. 5D**). Overall, these findings suggest a protumorigenic stromal phenotype which is characterized by increased CAFs, T-cell exhaustion, and high *SERPINE-1* and is associated with poor prognosis in colorectal cancer PM.

SERPINE-1 (*or PAI-1*) inhibition reverses EMT in colorectal cancer PM in a PAI-1–positive environment

Having identified *SERPINE-1*, also known as PAI-1, as a crucial target involved in transcoelomic metastasis, we sought to develop a PAI-1–neutralizing antibody as a potential therapeutic strategy for colorectal cancer PM.

Discovery of A5, a PAI-1–neutralizing antibody

A phage display was performed with a large human-naïve library of scFv by panning on a mixture of PAI-1 of active and latent conformations followed by screening for phages recognizing PAI-1

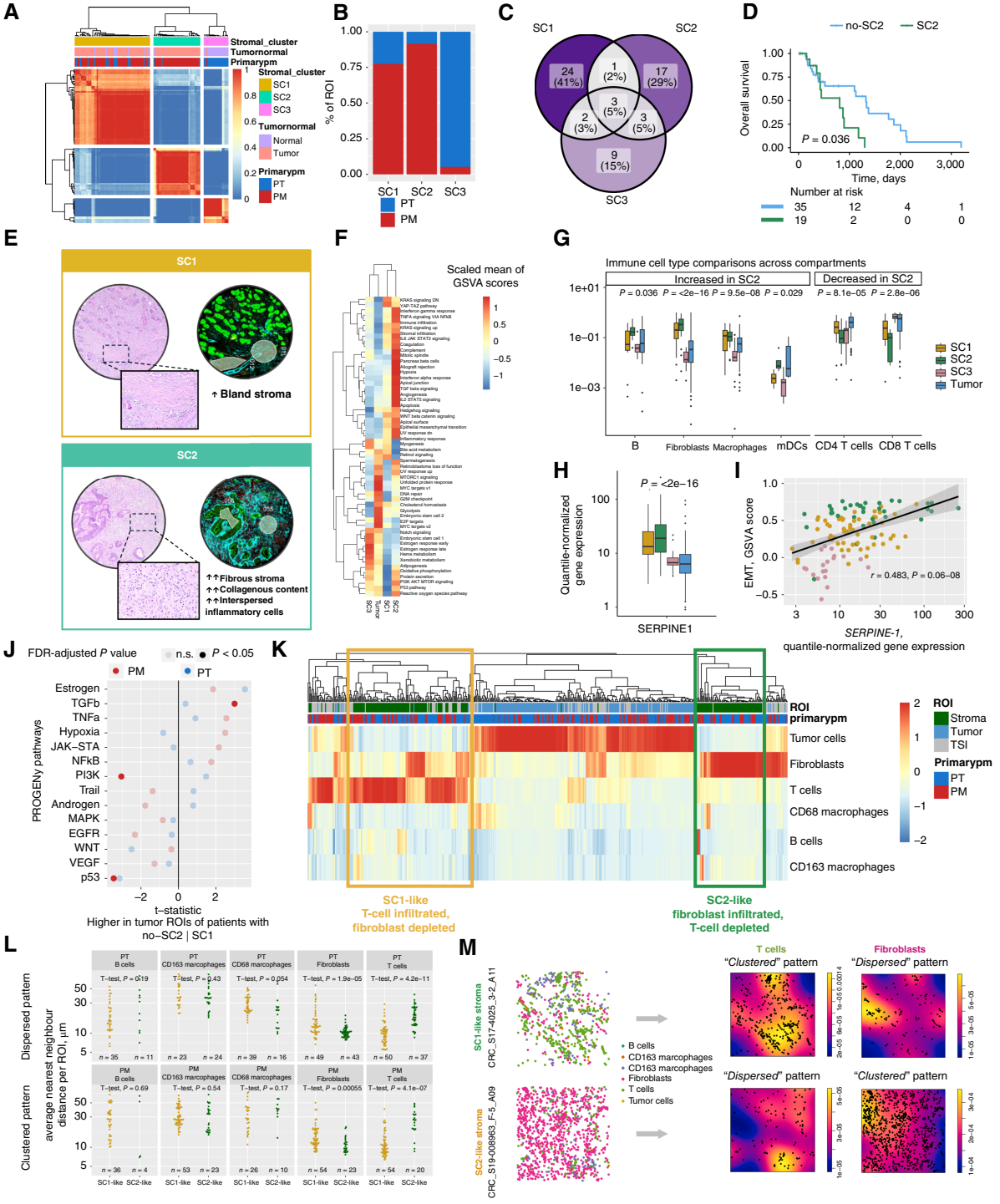

Figure 4.

Spatially revolved stromal phenotypes in CRC PM. **A,** Consensus clustering of stromal ROIs identifies three distinct stromal clusters. **B,** Proportion of stromal ROIs per stromal cluster stratified by the site of sample. **C,** Venn diagram depicting stromal cluster overlaps. **D,** Kaplan–Meier plot of overall survival stratified by stromal clusters (site agnostic). **E,** Stromal ROI H&E and DSP slides. **F,** Heatmap of pathway comparisons across compartments. **G,** SpatialDecon (31) immune cell type comparisons across compartments. **H,** *SERPINE-1* gene expression across compartments. **I,** Dotplot of *SERPINE-1* gene expression against EMT GSVA enrichment scores. **J,** Dotplot of PROGENy pathway comparisons between tumor compartments from patients with and without SC2. **K,** Heatmap of immune cell density from retrieved from mIHC (COMET, Lunaphore) across ROIs identifies two distinct stromal clusters consistent with DSP findings. **L,** Average immune cell type–specific nearest neighbor distance per stromal ROI stratified by immune cell types across PT vs. PM and stromal cluster. Only ROIs with >100 cells per immune cell type were included. **M,** Example reconstructed ROIs of SC1-like stroma (CRC_S17-4025_3-2_A11) and SC2-like stroma (CRC_S19-008963_F-5_A09) illustrating divergent spatial distributions of T cells and fibroblasts between stromal phenotypes. CRC, colorectal cancer; GSVA, gene set variation analysis.

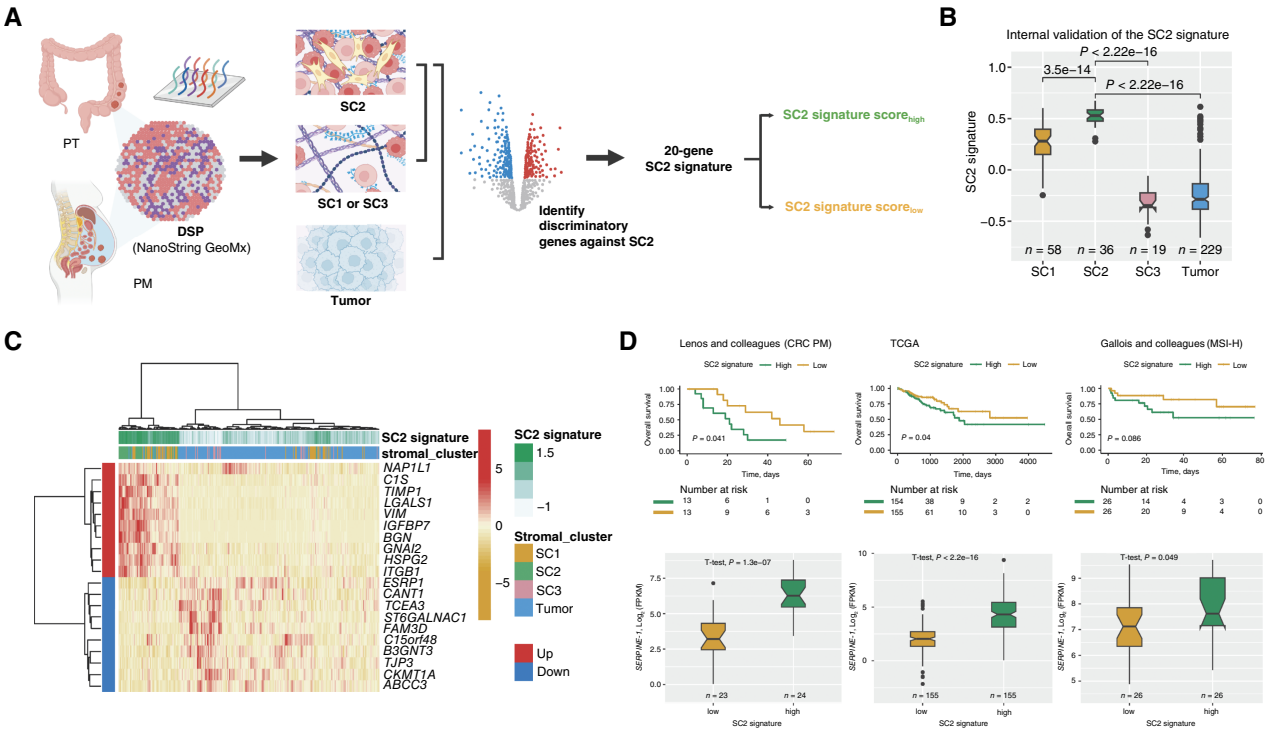

Figure 5.

Spatial distribution of SC2 cell types and development of an SC2 signature. **A,** Overview of the retrieval of SC2 signature score. **B,** Internal validation of the SC2 score on DSP data. **C,** Heatmap of SC2 signature genes across compartments. **D,** Overall survival Kaplan–Meier curves of other colorectal cohorts (Lenos and colleagues, TCGA, and Gallois and colleagues) and *SERPINE-1* gene expression stratified by SC2 signature (Q1 vs. Q4). For patients with multiple samples, the mean SC2 signature score was taken. GSVA, gene set variation analysis. [Created in BioRender. Sundar, R. (2025), https://BioRender.com/a03r463.]

using ELISA (**Fig. 6A**). Additionally, competitive ELISA was performed to select those capable of competing with PAI-1 small-molecule inhibitors (tiplaxtinin and TM5441). One scFv was selected for expression into IgG kappa format. This antibody, coined "A5," was able to recognize all wild-type active, wild-type latent, and stable active conformations of PAI-1 (**Fig. 6B**) and showed high binding affinity to three conformations of PAI-1 with KD at nanomolar ranges (Supplementary Table S6A). Furthermore, A5 neutralized PAI-1 functions in inhibiting tPA ($P = 0.0002$) and uPA (($P = 6.10e{-}04$) in chromogenic enzymatic assays (**Fig. 6C** and **D**). By utilizing NMR, we also found that A5 competes with the binding of tiplaxtinin to PAI-1, highlighting the binding affinity and potency of A5 compared with a known PAI-1 inhibitor (**Fig. 6D**).

Efficacy of A5 on colorectal cell lines in a PAI-1–positive environment

We investigated the efficacy of A5 in inhibiting PM cell proliferation in the presence of PAI-1–positive ascites *in vitro* by utilizing a cell line model representative of colorectal cancer PM, Colo-205 (Supplementary Table S6B). At a concentration of 150 μg/mL, A5 reduces proliferation of PM cells treated with seven PAI-1–positive ascites samples retrieved from patients with colorectal cancer PM in contrast to IgG controls (**Fig. 6E**). We further investigated the effects of the identified biologics on downstream pathways activated by PAI-1 in ascites and found that the treatment of A5 reduces the pSTAT3/STAT3 ratio in PM cancer cells treated with PAI-1–positive ascites from a patient with colorectal cancer PM (**Fig. 6F**). Next, we sought to investigate the effects of A5 on the transcriptome. Transcriptomes of Colo-205 PM cancer cells upon A5 treatment were profiled by RNA sequencing. Compared with cells treated with IgG, cells treated with A5 had reduced pathways such as IL2–STAT5, TGF-β, and IL6–JAK–STAT3 signaling (**Fig. 6G**).

Safety of systematic administration

In preparation for future human trials in which A5 is intended to be administered intraperitoneally to maximize its effect, we evaluated the safety of intravenous A5 administration in NCr nude mice. If A5 demonstrates safety when administered intravenously, we can reasonably conclude that it is unlikely to cause significant systemic toxicity when administered intraperitoneally even if some systemic absorption occurs. Into NCr nude mice, 50, 100, 150, and 200 μg A5 was administered ($n = 2$ female and 2 male mice for each dose) via intravenous injection. Bodyweight and behavior were assessed on a daily basis, followed by 16-hour fasting from day 13 before the final assessment of hematologic counts, clinical chemistry profiles, and pathologic evaluation (Supplementary Fig. S6A). The bodyweight of each mouse did not drop 14 days upon administration (Supplementary Fig. S6B and S6C). Counts of white blood cells, red blood cells, and platelets did not differ (Supplementary Fig. S6D–S6F). Clinical chemistry profiles of total protein, glucose, and albumin were comparable between A5 and PBS control (Supplementary Fig. S6G–S6I). Pathologic evaluation demonstrates

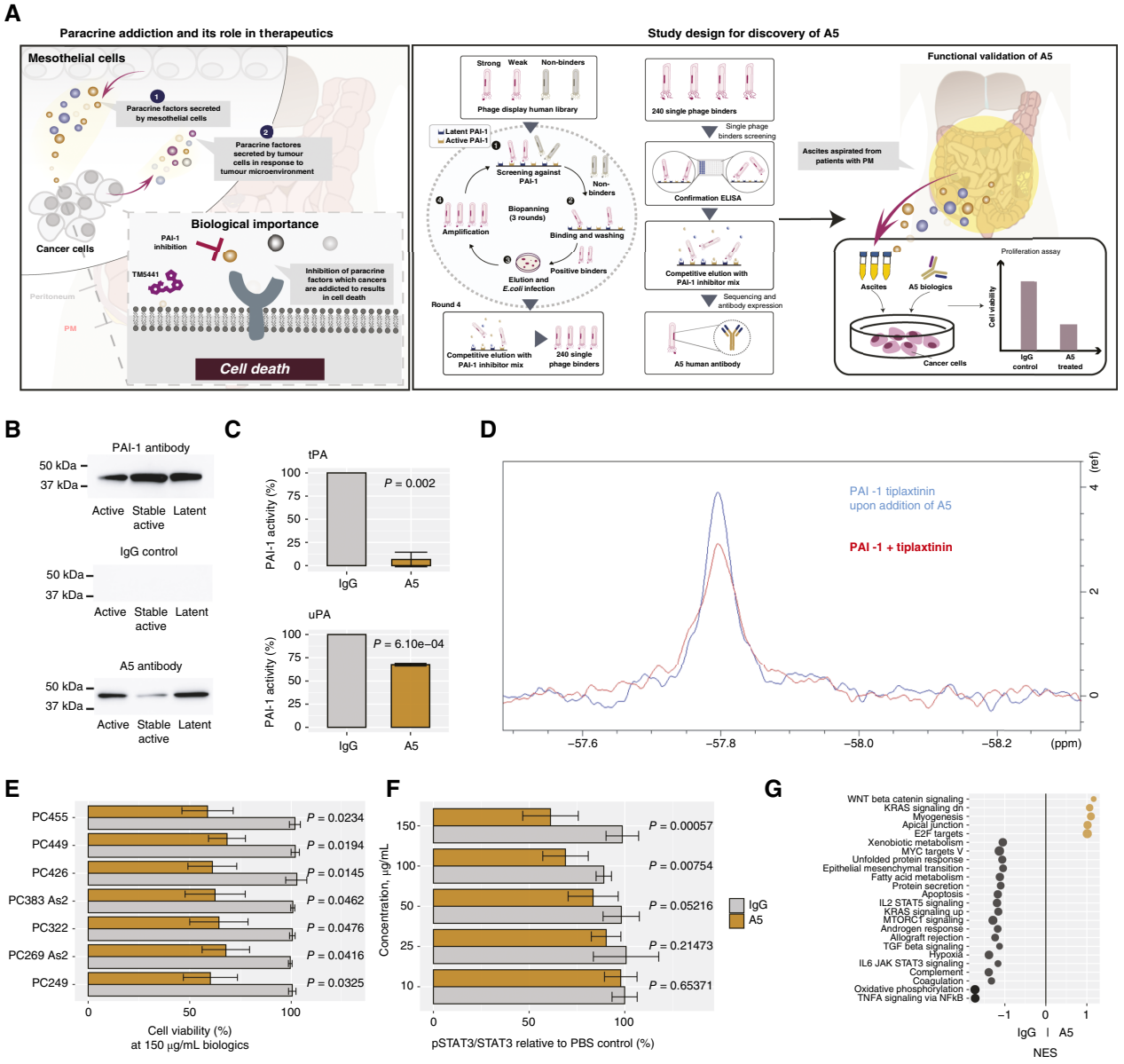

Figure 6.

Development of A5, a novel PAI-1–neutralizing antibody. **A,** Graphical illustration of phage screen and identification of PAI-1–neutralizing antibody. **B,** Recognition of different conformations of recombinant PAI-1 by A5 in Western blotting. **C,** A5 neutralized PAI-1 function in inhibiting tPA and uPA. **D,** Competitive binding of A5 with fluorine-containing tiplaxtinin on stable active PAI-1 assessed by 19F-NMR. **E,** Inhibition of proliferation of PM cells treated with PAI-1–positive ascites *in vitro* by 150 μg/mL A5 in biological triplicates. Human IgG served as a negative control. **F,** STAT3 signaling activation upon the exposure to PM ascites was suppressed by A5 as compared with IgG control. **G,** GSEA comparisons of HALLMARK pathway changes between CRC cells treated with A5 ($n = 2$) vs. IgG ($n = 2$). Pathways with an FDR adjusted P value of less than 0.05 are opacified. CRC, colorectal cancer; NES, normalized enrichment score.

intravenous administration of A5 at as high as 200 μg did not damage mice organs (Supplementary Table S6C). These data suggest that A5 is safe and unlikely to cause significant toxicity, even if it were to leak from the peritoneal cavity.

Discussion

To our knowledge, our study represents one of the first studies with a comprehensive multiomic analysis at spatial resolution of both PT and its paired PM tissue samples in the context of colorectal cancer PM. Distinctively, our research sets itself apart by revealing prognostically significant targets crucial for stroma–tumor interaction that hold potential for therapeutic exploitation. Combining CRS with HIPEC (38) marked a significant breakthrough in colorectal cancer PM treatment by directly targeting and resecting tumor lesions in the peritoneum (39). However, for patients unable to undergo surgery, systemic chemotherapy remains limited in its effectiveness (1). Patients with PM still present with poor response

to chemotherapy (1, 40), highlighting the urgent need for alternative therapeutic strategies in this sub-cohort of patients.

The dismal outlook of current non-surgical therapeutic strategies in colorectal cancer with PM amplifies the clinical significance of our study for its role in identifying potential therapeutic targets, unearthing the role of stroma in tumor progression. Current treatment modalities targeting tumor cells often fall short partly because cancers do not manifest disease progression alone; stroma–tumor interactions are also key drivers of tumor progression (41). In particular, the stroma environment facilitates tumor cell evolution and chemo-resistance, diminishing the efficacy of tumor cell–targeted treatments. For instance, some studies have demonstrated that in a cell-free ascites environment, the addition of tumor cell–specific therapy such as mitomycin C demonstrated resistance to the therapy (7). Hence, by homing in on specific paracrine targets, our study lays a crucial foundation for developing more effective treatments disrupting critical paracrine signaling pathways.

WES found that genomic alterations and clonality patterns between PTs and PMs remain broadly similar. In contrast, WTS showed clear differences between PT and PM samples. IL6–JAK–STAT3 signaling, TGF-β, and neovascularization were enhanced in PM. Differences in the composition of TME were also observed between PT and PM tumors in which PM demonstrated more macrophages and CAFs and lower plasma B cells and $CD4^+$ T cells; these findings corroborate with the existing pool of molecular studies (42). As tumor samples migrate to the peritoneum, they adopt a mesenchymal phenotype and fibrotic TME. We also studied putative tumor and immune gene targets of therapeutic significance involved in stroma–tumor communications in matched PT and PM samples. From the genes identified, we found *PAI-1* to be of prognostic significance, with patients having high *PAI-1* expression having poorer outcomes. With spatial profiling, we found that the tumor and stroma compartment make-up was more similar than thought to be between PT and PM. Findings on the similarities between the stroma compartment in PT and PM challenge existing notions of heterogeneity between PT and PM as seen in other types of cancer (43, 44).

Our study is not without its limitations. Although we performed WES, WTS, and spatial profiling of PT and matched PM samples, an in-depth analysis of other molecular characteristics such as proteomic and epigenomic studies of PT and PM samples would have provided another layer of insights into the multifaceted molecular landscape of colorectal cancer with PM. Demonstrating that introducing a PAI-1 inhibitor could lead to an improvement in patients with colorectal cancer PM would have further fortified our claim of PAI-1 as one of the cardinal factors mediating stroma–tumor communication and a viable therapeutic target. Notwithstanding, our previous study has notably demonstrated the therapeutic efficacy of PAI-1 inhibition through *in vitro* and *in vivo* mouse models (7). Upon introduction of PAI-1 inhibitor (TM5441) to PM cells *in vitro*, cells that were exposed to cell-free ascites with higher PAI-1 levels (>20 ng/mL) were more responsive to PAI-1 inhibition. Herein, we successfully illustrated the concept of paracrine addiction in peritoneal metastatic lesions and the profound impact of targeting paracrine signaling pathways in mitigating colorectal cancer with PM. We also illustrated that the administration of a PAI-1 biologic could be useful therapeutically through downregulation of key upstream pathways leading to EMT. In the pragmatic clinical setting, the use of biologics is potentially more desirable than small-molecule inhibitors, as the risk of systemic reabsorption through the peritoneal cavity is expected to be lower because of their larger size. Although PAI-1 is known to play a key role in fibrosis and extracellular matrix remodeling (45), and neutralizing it with A5 could potentially disrupt the fibrotic stroma to enhance drug penetration and immune response, *in vivo* studies are still needed. These studies will be crucial to determine whether PAI-1 inhibition can effectively penetrate and overcome the fibrotic and immune-suppressive stromal features characteristic of PMs, ultimately assessing its therapeutic potential within the complex TME.

Next, discrepancies in relative proportions of the site of origin were identified between stromal phenotypes between DSP and mIHC profiling approaches. In the DSP data, SC2 had a higher proportion of ROIs originating from PM samples. Conversely, in the mIHC data, the majority of SC2-like ROIs originated from PT. We cautioned on overinterpretation of these relative proportions, as ROIs were manually retrieved in both profiling methods, which may have introduced selection bias. Another limitation in this study is the absence of treatment data, including intra-peritoneal therapeutics such as HIPEC. Although incorporating such information could offer additional insights, its interpretation would be challenging given the variability in clinical contexts, as samples were retrieved for a range of reasons, including palliative and emergency surgeries. Furthermore, the survival benefit of CRS with HIPEC remains uncertain, with previous trials such as PRODIGE 7 (46) and PROPHYLOCHIP-PRODIGE 15 (47) showing no clear survival advantage. The complexity of HIPEC regimens and the lack of consensus on optimal chemotherapeutic agents further complicate efforts to assess its influence on clinical outcomes. Despite the absence of treatment data, our findings show that the SC2 stromal phenotype demonstrates consistent prognostic value across different stages, such as in TCGA, and was validated in an independent colorectal cancer PM dataset by Lenos and colleagues (20). This suggests that the poor prognostic impact of the SC2 phenotype is driven by its underlying biology rather than treatment effects.

In conclusion, we identified novel pro-tumorigenic therapeutic signatures governing stroma–tumor interactions. Our study identified and demonstrated the significant potential of PAI-1 as a viable biomarker in stroma-targeted therapy (48). To firmly establish stroma-targeted therapy in modern medicine, it is imperative to delineate other paracrine targets governing tumor–stroma cross-talk in colorectal cancer with PM. Exploring additional paracrine signatures may unveil a myriad of other targets, allowing us to fully realize the potential of stroma-targeted therapy. Our study heralds a new direction for modern cancer therapeutics in colorectal cancer PM, redefining the approach to treatment for this challenging disease.

Authors' Disclosures

C.-A.J. Ong reports a patent for 10202401700P pending. J.J. Zhao reports grants from National University Health System Seed Fund (NUHSRO/2024/008/RO5+6/Seed-Sep23/01), National University Hospital Junior Research Award 2023 (JRA/Sep23/002), Chan Heng Leong Education & Research Fund 2024 Award by the National University Hospital Singapore, 2025 Conquer Cancer Merit Award by Conquer Cancer, the ASCO Foundation, and Dean's Research Development Award awarded by the Yong Loo Lin School of Medicine, National University of Singapore, during the conduct of the study. Y. Liu reports a patent for 10202401700P pending. Q.X. Tan reports a patent for 10202401700P pending. J.W.S. Tan reports a patent for 10202401700P pending. J.-Y.J. Lee reports personal fees from National University Hospital (consultant) during the conduct of the study, as well as ImmunoQs (co-founder and COO). L.-H. Loo reports personal fees from National University Hospital (consultant) during the conduct of the study, as well as ImmunoQs (co-founder and CEO). C.Y.L. Chong reports a patent for 10202401700P pending. W. Guo reports a patent for 10202401700P pending. R.Y.K. Tay reports grants from the Clinician Scientist Development Unit (CSDU) NUS Medicine Student Research Mentorship Program. R. Walsh reports personal fees from Pfizer, Novartis, Merck, AstraZeneca, and Daiichi Sankyo outside the submitted work. F. Morano reports personal fees

from Pierre Fabre, Servier, and Accademia della Medicina, non-financial support from Pierre Fabre, Amgen, and AstraZeneca, and grants from Incyte outside the submitted work. L. Vermeulen reports employment with Genentech Inc. and ownership of Roche shares. M.F. Bijlsma reports grants from Celgene, Frame Therapeutics, Lead Pharma, and Wholomics and personal fees from Servier and Olympus outside the submitted work. S.J. Klempner reports personal fees from Astellas, Amgen, Merck, Bristol Myers Squibb, Daiichi Sankyo, AstraZeneca, Novartis, Elevation Oncology, Taiho, Gilead Sciences, BeiGene, Eisai, Natera, Sanofi-Aventis, Mersana, and I-Mab outside the submitted work. F. Pietrantonio reports grants from Amgen, Agenus, Eli Lilly and Company, AstraZeneca, Rottapharm, Bristol Myers Squibb, and Incyte and personal fees from BeiGene, Agenus, Gilead Sciences, Bristol Myers Squibb, MSD, AstraZeneca, Servier, Merck-Serono, Amgen, Bayer, Takeda, Pierre Fabre, Daiichi Sankyo, GSK, Ipsen, Johnson & Johnson, Jazz, Incyte, Astellas, Pfizer, and Italfarmaco outside the submitted work. R. Sundar reports grants from National Medical Research Council during the conduct of the study; personal fees and other support from Astellas, AstraZeneca, BeiGene, Bristol Myers Squibb, Daiichi Sankyo, DKSH, Ipsen, MSD, Roche, Taiho, and Teladoc; other support from Auristone, Bayer, CytoMed, Eisai, GSK, Merck, Natera, Novartis, Paxman Coolers, Pierre Fabre, Sanofi, and Tavotek BioTherapeutics; and personal fees from Eli Lilly and Company outside the submitted work; in addition, R. Sundar reports a patent for Auristone pending and a patent for Paxman Coolers pending. No disclosures were reported by the other authors.

Authors' Contributions

C.-A.J. Ong: Conceptualization, supervision, project administration, writing–review and editing. **J.J. Zhao:** Conceptualization, software, formal analysis, funding acquisition, investigation, visualization, methodology, writing–original draft, project administration, writing–review and editing. **Y. Liu:** Conceptualization, formal analysis, investigation, writing–original draft, writing–review and editing. **S. Srivasava:** Formal analysis, investigation, writing–review and editing. **D.K.A. Chia:** Formal analysis, investigation, writing–review and editing. **Y.E. Quek:** Formal analysis, investigation, writing–review and editing. **X. Fan:** Formal analysis, investigation, writing–review and editing. **H. Ma:** Formal analysis, investigation, writing–review and editing. **K.K. Huang:** Resources, data curation, formal analysis, investigation. **T. Sheng:** Resources, data curation, writing–review and editing. **Q.X. Tan:** Resources, data curation, writing–review and editing. **G. Ng:** Resources, data curation, writing–review and editing. **J.W.S. Tan:** Resources, data curation, writing–review and editing. **J.-Y.J. Lee:** Resources, data curation, writing–review and editing. **L.-H. Loo:** Writing–review and editing. **L.Y. Chong:** Writing–review and editing. **X.W. Ong:** Writing–review and editing. **S.T. Tay:** Writing–review and editing. **T. Hagihara:** Writing–review and editing. **A. Tan:** Writing–review and editing. **C.R.C. Joseph:** Writing–review and editing. **M.C.C. Teo:** Writing–review and editing. **J. Hendrikson:** Writing–review and editing. **C.Y.L. Chong:** Writing–review and editing. **W. Guo:** Writing–review and editing. **C.S. Chia:** Writing–review and editing. **J.S.M. Wong:** Writing–review and editing. **C.J. Seo:** Writing–review and editing. **M. Cai:** Writing–review and editing. **Y. Tay:** Writing–review and editing. **K.M.S. Sim:** Writing–review and editing. **R.Y.K. Tay:** Writing–review and editing. **R. Walsh:** Writing–review and editing. **M. Guaglio:** Writing–review and editing. **F. Morano:** Writing–review and editing. **M. Teh:** Writing–review and editing. **H.Y.J. Lum:** Writing–review and editing. **T.K.H. Lim:** Writing–review and editing. **L. Vermeulen:** Writing–review and editing. **M.F. Bijlsma:** Writing–review and editing. **K. Lenos:** Writing–review and editing. **S.J. Klempner:** Writing–review and editing. **J.P.S. Yeong:** Data curation, investigation, writing–review and editing. **W.P. Yong:** Data curation, investigation, writing–review and editing. **F. Pietrantonio:** Resources, data curation, investigation, writing–review and editing. **P. Tan:** Resources, data curation, supervision, project administration, writing–review and editing. **R. Sundar:** Conceptualization, resources, data curation, supervision, investigation, project administration, writing–review and editing.

Acknowledgments

C.-A.J. Ong is supported by the National Medical Research Council Clinician Scientist-Individual Research Grants (MOH-CIRG21jun-0005 and MOH-CIRG24jan-0044), Clinician Scientist Award (INV category; MOH-CSAINV22jul-0005), and Singapore Ministry of Health's National Medical Research Council under its Open Fund-Large Collaborative Grant ("OF-LCG"; MOH-OFLCG18-May-0003 and MOH-OFLCG23-may0031). J.-Y.J. Lee and J.J. Zhao are supported by the National University Health System Seed Fund (NUHSRO/2024/008/RO5+6/Seed-Sep23/01), National University Hospital Junior Research Award 2023 (JRA/Sep23/002), Chan Heng Leong Education & Research Fund 2024 award by the National University Hospital Singapore, 2025 Conquer Cancer Merit Award by Conquer Cancer, the ASCO Foundation, and Dean's Research Development Award awarded by the Yong Loo Lin School of Medicine, National University of Singapore. J.-Y.J. Lee is supported by the National Medical Research Council Open Fund-Young Investigator Award (MOH-OFYIRG24jan-0052). D.K.A. Chia is supported by the ExxonMobil-NUS Research Fellowship, the National University Health System (NUHSRO/2022/057/RO5+6/Seed-Mar/02), and the National Medical Research Council (NMRC/RTF/MH 095:003\008-332). R.Y.K. Tay is supported by the Clinician Scientist Development Unit (CSDU) NUS Medicine Student Research Mentorship Program. F. Morano Federica received research funding (to institution) from Incyte. S.J. Klempner is supported by the Dana-Farber/Harvard Cancer Center (DF/HCC) Specialized Program in Research Excellence (SPORE) in Gastrointestinal Cancer Developmental Research Project (DRP) dispersed from the parent NIH GI SPORE award 2P50CA127003. F. Pietrantonio is supported by AIRC (Associazione Italiana per la Ricerca sul Cancro), IG 2019 number 23624, and Italian Ministry of Health GR-2019-12371132. P. Tan's research was supported by the National Research Foundation, Singapore, and Singapore Ministry of Health's National Medical Research Council under its Open Fund-Large Collaborative Grant ("OF-LCG"; MOH-OFLCG18-May-0003) and the Singapore Gastric Cancer Consortium. His work was also supported by the National Medical Research Council grant MOH-000967. R. Sundar is supported by the National Medical Research Council (NMRC/CIRG23Jul-0035 and NMRC/MOH-000627). All other authors do not have any funding sources to declare. This work was supported by the A*STAR Biomedical Engineering Programme (C211318003), Singapore National Medical Research Council (MOH-000323-00, OFYIRG19may-0007), Industry Alignment Fund-Industry Collaboration Fund (IAF-ICP I2201E0014), and A*STAR I&E GAP Fund (I24D1AG082). The other funders of the study had no role in study design, data collection, analysis, interpretation, or writing of the manuscript.

Note

Supplementary data for this article are available at Clinical Cancer Research Online (http://clincancerres.aacrjournals.org/).

Received November 11, 2024; revised January 17, 2025; accepted April 9, 2025; posted first April 29, 2025.

References

1. Franko J, Shi Q, Meyers JP, Maughan TS, Adams RA, Seymour MT, et al. Prognosis of patients with peritoneal metastatic colorectal cancer given systemic therapy: an analysis of individual patient data from prospective randomised trials from the Analysis and Research in Cancers of the Digestive System (ARCAD) database. Lancet Oncol 2016;17:1709–19.
2. Lemoine L, Sugarbaker P, Van der Speeten K. Pathophysiology of colorectal peritoneal carcinomatosis: role of the peritoneum. World J Gastroenterol 2016;22:7692–707.
3. Tommelein J, Verset L, Boterberg T, Demetter P, Bracke M, De Wever O. Cancer-associated fibroblasts connect metastasis-promoting communication in colorectal cancer. Front Oncol 2015;5:63.
4. Kalluri R. The biology and function of fibroblasts in cancer. Nat Rev Cancer 2016;16:582–98.
5. Monteran L, Zait Y, Erez N. It's all about the base: stromal cells are central orchestrators of metastasis. Trends Cancer 2024;10:208–29.
6. Zhao JJ, Ong C-AJ, Srivastava S, Chia DKA, Ma H, Huang K, et al. Spatially resolved niche and tumor microenvironmental alterations in gastric cancer peritoneal metastases. Gastroenterology 2024;167:1384–98.e4.
7. Hendrikson J, Liu Y, Ng WH, Lee JY, Lim AH, Loh JW, et al. Ligand-mediated PAI-1 inhibition in a mouse model of peritoneal carcinomatosis. Cell Rep Med 2022;3:100526.
8. Zhan HX, Zhou B, Cheng YG, Xu JW, Wang L, Zhang GY, et al. Crosstalk between stromal cells and cancer cells in pancreatic cancer: new insights into stromal biology. Cancer Lett 2017;392:83–93.

9. Erkan M, Hausmann S, Michalski CW, Fingerle AA, Dobritz M, Kleeff J, et al. The role of stroma in pancreatic cancer: diagnostic and therapeutic implications. Nat Rev Gastroenterol Hepatol 2012;9:454–67.
10. Chen Y, Cai G, Jiang J, He C, Chen Y, Ding Y, et al. Proteomic profiling of gastric cancer with peritoneal metastasis identifies a protein signature associated with immune microenvironment and patient outcome. Gastric Cancer 2023;26:504–16.
11. Lawler M, Alsina D, Adams RA, Anderson AS, Brown G, Fearnhead NS, et al. Critical research gaps and recommendations to inform research prioritisation for more effective prevention and improved outcomes in colorectal cancer. Gut 2018;67:179–93.
12. Sasaki T, Nakamura T, Rebhun RB, Cheng H, Hale KS, Tsan RZ, et al. Modification of the primary tumor microenvironment by transforming growth factor alpha-epidermal growth factor receptor signaling promotes metastasis in an orthotopic colon cancer model. Am J Pathol 2008;173:205–16.
13. Li H, Durbin R. Fast and accurate short read alignment with Burrows-Wheeler transform. Bioinformatics 2009;25:1754–60.
14. Cibulskis K, Lawrence MS, Carter SL, Sivachenko A, Jaffe D, Sougnez C, et al. Sensitive detection of somatic point mutations in impure and heterogeneous cancer samples. Nat Biotechnol 2013;31:213–9.
15. Mayakonda A, Lin DC, Assenov Y, Plass C, Koeffler HP. Maftools: efficient and comprehensive analysis of somatic variants in cancer. Genome Res 2018;28:1747–56.
16. Li B, Dewey CN. RSEM: accurate transcript quantification from RNA-seq data with or without a reference genome. BMC Bioinformatics 2011;12:323.
17. Monti S, Tamayo P, Mesirov J, Golub T. Consensus clustering: a resampling-based method for class discovery and visualization of gene expression microarray data. Mach Learn 2003;52:91–118.
18. Xu T, Le TD, Liu L, Su N, Wang R, Sun B, et al. CancerSubtypes: an R/Bioconductor package for molecular cancer subtype identification, validation and visualization. Bioinformatics 2017;33:3131–3.
19. Foroutan M, Bhuva DD, Lyu R, Horan K, Cursons J, Davis MJ. Single sample scoring of molecular phenotypes. BMC Bioinformatics 2018;19:404.
20. Lenos KJ, Bach S, Ferreira Moreno L, ten Hoorn S, Sluiter NR, Bootsma S, et al. Molecular characterization of colorectal cancer related peritoneal metastatic disease. Nat Commun 2022;13:4443.
21. Stein MK, Williard FW, Xiu J, Tsao MW, Martin MG, Deschner BW, et al. Comprehensive tumor profiling reveals unique molecular differences between peritoneal metastases and primary colorectal adenocarcinoma. J Surg Oncol 2020;121:1320–8.
22. Househam J, Heide T, Cresswell GD, Spiteri I, Kimberley C, Zapata L, et al. Phenotypic plasticity and genetic control in colorectal cancer evolution. Nature 2022;611:744–53.
23. Hu Z, Curtis C. Looking backward in time to define the chronology of metastasis. Nat Commun 2020;11:3213.
24. Malagoli Tagliazucchi G, Wiecek AJ, Withnell E, Secrier M. Genomic and microenvironmental heterogeneity shaping epithelial-to-mesenchymal trajectories in cancer. Nat Commun 2023;14:789.
25. Yoshihara K, Shahmoradgoli M, Martínez E, Vegesna R, Kim H, Torres-Garcia W, et al. Inferring tumour purity and stromal and immune cell admixture from expression data. Nat Commun 2013;4:2612.
26. Guinney J, Dienstmann R, Wang X, de Reyniès A, Schlicker A, Soneson C, et al. The consensus molecular subtypes of colorectal cancer. Nat Med 2015;21:1350–6.
27. Eide PW, Bruun J, Lothe RA, Sveen A. CMScaller: an R package for consensus molecular subtyping of colorectal cancer pre-clinical models. Sci Rep 2017;7:16618.
28. Bagaev A, Kotlov N, Nomie K, Svekolkin V, Gafurov A, Isaeva O, et al. Conserved pan-cancer microenvironment subtypes predict response to immunotherapy. Cancer Cell 2021;39:845–65.e7.
29. Wang S, Pang L, Liu Z, Meng X. SERPINE1 associated with remodeling of the tumor microenvironment in colon cancer progression: a novel therapeutic target. BMC Cancer 2021;21:767.
30. Cambria E, Coughlin MF, Floryan MA, Offeddu GS, Shelton SE, Kamm RD. Linking cell mechanical memory and cancer metastasis. Nat Rev Cancer 2024;24:216–28.
31. Danaher P, Kim Y, Nelson B, Griswold M, Yang Z, Piazza E, et al. Advances in mixed cell deconvolution enable quantification of cell types in spatial transcriptomic data. Nat Commun 2022;13:385.
32. Kieffer Y, Hocine HR, Gentric G, Pelon F, Bernard C, Bourachot B, et al. Single-cell analysis reveals fibroblast clusters linked to immunotherapy resistance in cancer. Cancer Discov 2020;10:1330–51.
33. Dybkær K, Bøgsted M, Falgreen S, Bødker JS, Kjeldsen MK, Schmitz A, et al. Diffuse large B-cell lymphoma classification system that associates normal B-cell subset phenotypes with prognosis. J Clin Oncol 2015;33:1379–88.
34. Newman AM, Liu CL, Green MR, Gentles AJ, Feng W, Xu Y, et al. Robust enumeration of cell subsets from tissue expression profiles. Nat Methods 2015;12:453–7.
35. Jiang P, Gu S, Pan D, Fu J, Sahu A, Hu X, et al. Signatures of T cell dysfunction and exclusion predict cancer immunotherapy response. Nat Med 2018;24:1550–8.
36. Cancer Genome Atlas Research Network; Weinstein JN, Collisson EA, Mills GB, Shaw KRM, Ozenberger BA, Ellrott K, et al. The Cancer Genome Atlas Pan-Cancer analysis project. Nat Genet 2013;45:1113–20.
37. Gallois C, Landi M, Taieb J, Sroussi M, Saberzadeh-Ardestani B, Cazelles A, et al. Transcriptomic signatures of MSI-high metastatic colorectal cancer predict efficacy of immune checkpoint inhibitors. Clin Cancer Res 2023;29:3771–8.
38. Sugarbaker PH. Carcinoma of the colon—prognosis and operative choice. Curr Probl Surg 1981;18:753–802.
39. Verwaal VJ, van Ruth S, de Bree E, van Sloothen GW, van Tinteren H, Boot H, et al. Randomized trial of cytoreduction and hyperthermic intraperitoneal chemotherapy versus systemic chemotherapy and palliative surgery in patients with peritoneal carcinomatosis of colorectal cancer. J Clin Oncol 2003;21:3737–43.
40. Franko J, Shi Q, Goldman CD, Pockaj BA, Nelson GD, Goldberg RM, et al. Treatment of colorectal peritoneal carcinomatosis with systemic chemotherapy: a pooled analysis of north central cancer treatment group phase III trials N9741 and N9841. J Clin Oncol 2012;30:263–7.
41. de Visser KE, Joyce JA. The evolving tumor microenvironment: from cancer initiation to metastatic outgrowth. Cancer Cell 2023;41:374–403.
42. Demuytere J, Ernst S, van Ovost J, Cosyns S, Ceelen W. The tumor immune microenvironment in peritoneal carcinomatosis. Int Rev Cell Mol Biol 2022;371:63–95.
43. Klaver YL, Simkens LH, Lemmens VE, Koopman M, Teerenstra S, Bleichrodt RP, et al. Outcomes of colorectal cancer patients with peritoneal carcinomatosis treated with chemotherapy with and without targeted therapy. Eur J Surg Oncol 2012;38:617–23.
44. Valiente M, Ahluwalia MS, Boire A, Brastianos PK, Goldberg SB, Lee EQ, et al. The evolving landscape of brain metastasis. Trends Cancer 2018;4:176–96.
45. Ghosh AK, Vaughan DE. PAI-1 in tissue fibrosis. J Cell Physiol 2012;227:493–507.
46. Quénet F, Elias D, Roca L, Goéré D, Ghouti L, Pocard M, et al. Cytoreductive surgery plus hyperthermic intraperitoneal chemotherapy versus cytoreductive surgery alone for colorectal peritoneal metastases (PRODIGE 7): a multicentre, randomised, open-label, phase 3 trial. Lancet Oncol 2021;22:256–66.
47. Goéré D, Glehen O, Quenet F, Guilloit J-M, Bereder J-M, Lorimier G, et al. Second-look surgery plus hyperthermic intraperitoneal chemotherapy versus surveillance in patients at high risk of developing colorectal peritoneal metastases (PROPHYLOCHIP–PRODIGE 15): a randomised, phase 3 study. Lancet Oncol 2020;21:1147–54.
48. Li R, Liu X, Huang X, Zhang D, Chen Z, Zhang J, et al. Single-cell transcriptomic analysis deciphers heterogenous cancer stem-like cells in colorectal cancer and their organ-specific metastasis. Gut 2024;73:470–84.